Indian Journal of Chemical Technology
Vol. 33, July 2026, pp. 574-585
DOI: 10.56042/ijct.v33i4.27877

Enhanced cooling dynamics in slip-induced MHD Williamson nanofluid flow under thermal stratification

K. Anantha Kumar[1]* & N. Sandeep[2]

[1]Department of Mathematics, Sri Venkateswara College of Engineering, Karakambadi, Tirupati, AP, India
[2]Department of Mathematics, Central University of Karnataka, Kalaburagi, Karnataka, India

*E-mail: ananth.svu@gmail.com

Received 23 January 2026; accepted 1 July 2026

The present investigation explores thermal transport characteristics in MHD Williamson nanofluid flowing over a permeable stretching surface subjected to velocity and thermal slip boundary conditions. Thermal stratification, Ohmic dissipation, and internal heat source/sink effects are embedded into the governing mathematical framework to reflect practical engineering scenarios. An aqueous suspension of silver nanoparticles (Ag–H_2O) serves as the working nanofluid throughout this analysis. Appropriate similarity variables are applied to reduce the nonlinear governing PDEs to a coupled ODE system, which is subsequently integrated numerically via the fourth-order Runge–Kutta shooting algorithm implemented in MATLAB. The numerical outcomes reveal that intensifying the applied magnetic field decelerates the fluid motion while simultaneously elevating temperatures across the thermal boundary layer. An increase in thermal stratification diminishes the wall temperature gradient, consequently leading to a reduction in the convective heat transfer rate at the surface. Incorporating silver nanoparticles into the base fluid markedly enhances the effective thermal conductivity and modifies the momentum profiles, yielding a substantial improvement in overall heat transfer efficiency. The findings underscore the practical relevance of Williamson nanofluids in electromagnetic flow regulation and precision cooling systems, spanning aerospace thermal management, high-performance electronics, biomedical instrumentation, and industrial manufacturing operations.

Keywords*:* Convection, Joule heating, Heat source/sink, Shear thickening fluid, Thermic heat

Introduction

The Williamson constitutive model provides an accurate mathematical representation of shear-thinning rheology encountered across a broad spectrum of industrial processes and physiological flow systems. The characteristic reduction in apparent viscosity with rising shear rate renders these fluids highly amenable to flow regulation in dynamically varying operational environments. Suspension of metallic or oxide nanoparticles in such fluids substantially elevates the effective thermal conductivity, thereby accelerating heat dissipation rates. Such nanofluids find extensive utilisation in industrial operations including polymeric extrusion, surface coating processes, and catalytic reactors dealing with shear-sensitive media. Within biomedical contexts, Williamson-type fluids offer a physiologically relevant framework for simulating haemodynamic behaviour and facilitating controlled pharmaceutical transport. Beyond these domains, Williamson nanofluids are actively investigated for thermal management in compact electronics, concentrated solar collectors, geothermal energy recovery units, and tribological systems demanding superior lubrication and heat dissipation. Akbar *et al*.[1] probed Williamson liquid stream over an exponentially stretched sheet and found improved heat conduction influenced by pseudoplastic properties, which is beneficial for stretchable materials and industrial extrusion. Zeeshan and Ellahi[2] demonstrated that hybrid nanofluids containing alumina–copper nanoparticles improve heat transfer performance under slip and magnetic effects, showing promise for cooling systems in compact thermal devices. Olkha and Kumar[3] analyzed a vertical configuration involving hybrid Williamson nanofluids and reported an enhanced Nusselt number, suggesting its viability for energy-efficient thermal exchangers. Arain *et al*.[4] applied a semi-analytical approach to reveal that radiative nanoparticle-coated flows in confined cavities increase localized heat transfer, supporting applications in thermal optimization of solar units and chip-level cooling. Abbas *et al*.[5] studied Joule heating in thermally stratified Williamson nanofluid flows and related the findings to layered conductive polymers and functional fluidic architectures. Ashwinkumar[6] analyzed unsteady MHD nanoliquid flow over an elongated surface in 2021, showing enhanced heat and mass transfer performance. Later, Sulochana *et al*.[7] investigated Joule heating effects in MgO–CuO mixed nanofluids, highlighting improved thermal transport characteristics. Kumar *et al*.[8] extended this understanding by examining magnetized Casson nanofluids in porous settings, finding relevance for geothermal recovery systems and subsurface heat storage platforms. Most recently, Ashwinkumar[9] studied the MHD Sakiadis flow of hybrid nanoliquids past a continuously moving thin needle, reporting strengthened heat transfer under magnetic influence. The study concluded that incorporating hybrid nanoliquids under magnetic fields significantly improves the thermal performance and can be effectively applied to enhance heat transfer in engineering applications.

Electromagnetic coupling in Williamson nanofluids assumes critical significance in technologically demanding environments, notably plasma confinement reactors, molten-metal processing units, and fusion energy extraction systems, where Lorentz body forces govern fluid dynamics. The intrinsic magneto-sensitivity of these fluids, combined with their non-Newtonian constitutive behaviour, enables precise manipulation in MHD power generators, magnetically guided therapeutic delivery systems, and reactor wall thermal protection circuits. Furthermore, externally imposed magnetic regulation serves to stabilise laminar flow structures, attenuate turbulent fluctuations, promote uniform temperature distribution, and optimise energy utilisation across advanced thermal engineering and materials processing platforms. Mondal *et al*.[10] demonstrated that magnetic forces elevate entropy production and dampen convection in porous geometries, facilitating innovation in thermal insulation frameworks for porous components. Raju and Sandeep[11] explored how Joule heating and viscous dissipation reshape thermal and velocity gradients in MHD Williamson fluids, contributing insights for electro-thermal manufacturing and small-scale energy harvesters. Rasool *et al*.[12] obsessed on Hall currents, drag, and biological response effects on MHD shear thickening nanofluid stream, revealing that Lorentz forces and reactive transport significantly alter flow and thermal fields, an effect critical for advanced microelectronic thermal systems. Khan *et al*.[13] showed that magnetic field interaction with Joule heating heightens irreversibility in these fluids, with implications for spacecraft surface protection and magnetic fluid control in biomedical platforms. Sharma *et al*.[14] reported synergistic effects of entropy generation in Williamson nanofluid flows, providing a holistic view on fluid irreversibility under electromagnetic and radiative influence. Sandeep *et al*.[15] emphasized the role of nanolayers in boosting thermal conductivity for solar-based energy systems, highlighting that the presence of nanoscale structures not only enhances heat transfer but also improves the magneto-hydrodynamic (MHD) response, allowing better control of flow and thermal distribution under electromagnetic influence.

Thermal radiation exerts a pronounced influence on heat transport in non-Newtonian nanofluids, critically affecting system performance in solar energy conversion devices, aerospace thermal protection systems, and laser-driven thermal processing applications. This radiation–convection interaction becomes especially consequential in extreme-temperature operating conditions encountered in gas turbine stages, atmospheric re-entry capsules, high-flux solar concentrators, and precision manufacturing environments demanding stringent temperature control. Through augmenting both energy absorption capacity and heat rejection pathways, radiative contributions collectively elevate operational efficiency, thermal stability, and system reliability in contemporary thermal engineering infrastructure. Sheikholeslami and Ganji[16] demonstrated that the interplay of thermal radiation and magnetic fields influences convection characteristics in non-Newtonian nanofluids, relevant for radiation-intensive enclosures and high-altitude aerodynamics. Sulochana and Ashwinkumar[17] investigated MHD flow of magnetic nanofluids past an elongated sheet, focusing on the roles of Brownian motion and thermophoresis along with thermal diffusion. They found that the combined influence of Brownian motion and thermophoresis notably increases the rate of heat transfer under a magnetic field. Ashwinkumar and Sulochana[18] studied mixed convection MHD flow of Casson nanofluids containing $Al_{50}Cu_{50}$ alloy nanoparticles, considering radiation absorption and buoyancy effects. Their analysis revealed that both radiation absorption and buoyancy significantly enhance radiative heat transfer in these nanofluid flows. Lone *et al*.[19] compared hybrid and mono nanofluids, finding enhanced radiative-conductive synergy in hybrids suitable for photovoltaic panel cooling and thermal coatings under concentrated radiation. Nisar *et al*.[20] revealed that bioconvective Sisko nanofluid flow is significantly impacted by Joule heating and radiation, offering implications for thermal regulation in diagnostic microfluidics and biomedical microchannels. El-Hakiem *et al*.[21] analyzed MHD shear thickening nanofluid flow under velocity and thermal slip with radiation in porous media, highlighting benefits for thermal insulation coatings in aerospace structures. Rashad *et al*.[22] investigated hybrid Williamson nanofluids subjected to nonlinear thermal radiation and Ohmic heating, showing that increased radiative effects raise the fluid temperature, thereby improving heat retention in reactive and high-temperature containment systems used in advanced thermal technologies.

Thermal stratification and spatially distributed heat generation or absorption represent fundamental phenomena governing transport in nanofluids, particularly in configurations exhibiting naturally occurring temperature layering or localised thermal excitation. Such effects carry direct implications for environmental thermal modelling, layered industrial energy systems, and thermally active storage vessels with embedded heating elements. Precise management of internal heat source or sink intensity is indispensable in nuclear reactor thermal circuits, exothermic reaction processing, chip-level electronic cooling architectures, and latent heat energy storage systems, where uniform and stable thermal fields are prerequisites for operational safety, process efficiency, and component longevity. Rawat *et al*.[23] correlated spatial variations in internal heat generation with radiative heat transfer behaviour, offering insights for next-generation solar heating systems. Yasmin *et al*.[24] investigated ternary hybrid nanofluid flows and highlighted the influence of convection and slip situations under radiative effects, relevant for layered multi-fluid cooling arrangements. Kayalvizhi and Kumar[25] noted that electromagnetohydrodynamic and radiative effects in hybrid nanofluids significantly alter entropy generation near stagnation zones, a condition frequently encountered in rotary thermal devices and disk-based absorbers. Kazmi *et al*.[26], using inclined magnetic fields and peristaltic flows, connected entropy variations to magnetic nanoparticle motion, suggesting roles in smart thermal filtration and predictive heat control systems. Shah *et al*.[27] examined chemical reactions and activation energy in radiative MHD nanofluid flows, further underscoring the role of thermal layering and viscous dissipation in energy transport regulation.

At microscale dimensions, the departure from classical no-slip and no-jump boundary conditions substantially alters fluid transport characteristics, a consideration of paramount importance in microelectro-mechanical systems (MEMS), microfluidic lab-on-chip platforms, and nanoscale thermal management networks. The dominance of surface-to-volume effects in microscale configurations renders slip phenomena especially consequential in catalytic microreactors, biomedical point-of-care diagnostic devices, miniaturised heat exchangers, and ultra-dense electronic packaging modules. Faithful incorporation of velocity and thermal slip conditions into the governing equations therefore substantially improves predictive fidelity and underpins more effective design methodologies for miniaturised thermal-fluidic devices. Shah *et al*.[28] reported that incorporating velocity slip under radiation conditions improves heat conduction in MHD Maxwell nanofluid flow over inclined geometries, relevant for precision fluidic heat exchangers. Abbas *et al*.[29] analyzed slip-influenced heat and momentum transfer in dissipative micropolar fluids, revealing strong alterations in wall heat flux, a concern for magneto-fluidic controllers and micro-scale heat sensors. Akbar *et al*.[30] examined slip in both Carreau and Williamson nanofluids and identified secondary flow development that affects localized heat dissipation, with applications in micro-spinning heat extraction units. Anantha Kumar *et al*.[31,32] found that thermal slip enhances heat and mass transport in vertical configurations with hybrid nanofluids under Joule heating, informing the design of stacked electronic component cooling arrays and vertical energy converters. Raju *et al*.[33] explored how slip and Joule heating synergistically boost heat transfer in vertical flows, offering engineering designs for energy-efficient vertical heat exchangers. Sandeep *et al*.[34] analyzed cylindrical film flow of Prandtl ferrofluids using Hamilton-Crosser and Xue nano models, demonstrating that optimized nanofluid formulations can significantly improve solar energy utilization and enhance thermal performance in thin-film flow systems.

Notwithstanding the considerable volume of existing research on non-Newtonian nanofluids, investigations have predominantly examined isolated physical mechanisms including magnetic interaction, radiative transfer, Ohmic heating, or boundary slip rather than their simultaneous interplay. Studies addressing the concurrent action of MHD, thermal stratification, radiation, internal heat source/sink effects, and slip conditions in Williamson nanofluids remain conspicuously scarce, despite the engineering relevance of such coupled configurations. The translational potential of such multi-physics frameworks for aerospace heat shielding, electronic thermal management, biomedical flow devices, and stratified energy storage architectures likewise warrants more systematic investigation.

The current work bridges this research gap by formulating the boundary layer flow over a stretching permeable surface, reducing the governing PDEs through similarity variable substitution, and obtaining numerical solutions via the fourth-order Runge–Kutta shooting method in MATLAB. Principal engineering quantities i.e., the dimensionless velocity field, temperature distribution, skin friction coefficient, and Nusselt number are systematically examined using graphical profiles and tabulated comparative data. The results yield novel quantitative insights applicable to optimised thermal management strategies, precision cooling circuit design, and next-generation energy conversion device engineering.

Formulation

The present study examines a two-dimensional shear-thickening stratified nanofluid flow induced by a stretching surface under the influence of internal heat generation or absorption. The fluid occupies the region $y > 0$, with the Cartesian coordinate system defined as (x, y). The stream is steady and not turbulent. Along the *x*-direction, the stretching velocity is $u_w(x) = ax$ as styled in the subsequent study. A constant magnetic fore of strength B_0 is smeared perpendicular to the stream way as revealed in Fig. 1.

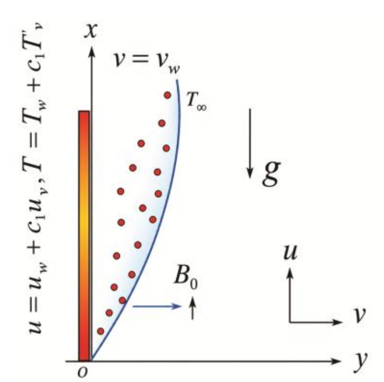

Fig. 1 — Flow geometry

The relevant mathematical model describing the conduct of Williamson nanofluid flow is established over the transformation of the fundamental conservation equations to align with the specified boundary-layer assumptions[16,37].

$$u_x + v_y = 0 \quad \ldots(1)$$

$$\rho_{nf}\left(uu_x + vu_y\right) = \mu_{nf}\left(1 + \sqrt{2}\Gamma u_y\right)u_{yy} - u\frac{\mu_{nf}}{K_0} + (\rho\beta)_{nf}\, g(T - T_\infty) + \sigma_{nf} {B_0}^2 u \quad \ldots(2)$$

$$\left(\rho c_p\right)_{nf}\left(u\,T_x + v\,T_y\right) = k_{nf}\left(1 + 16\frac{\sigma^* T_\infty^3}{3k_f k^*}\right)T_{yy} + Q_*(T - T_\infty) + \sigma_{nf} {B_0}^2 u^2 - S_T u \quad \ldots(3)$$

Since, $S_T = \frac{\partial T_\infty}{\partial x} + \frac{g}{C_p}$ signifies the stratified factor, where the rate of reversible work i.e. $\frac{g}{C_p}$ is assumed to be negligible.

Boundary conditions[16,37]

$$\left.\begin{array}{c} u = u_w + c_1 u_y\,, v = v_w, T = T_w + c_2 T_y \text{ at } y = 0 \\ u \to 0, T \to T_\infty \text{ as } y \to \infty \end{array}\right\} \quad \ldots(4)$$

Similarity transformation variables

$$u = ax\,f', v = -\sqrt{a\,\nu_f}\,f, T - T_\infty = (T_w - T_\infty)\theta, \eta = \sqrt{\frac{a}{\nu_f}}\,y \quad \ldots(5)$$

Thermic features of nanofluid are as follows[37].

Qualities	Nanofluid
Viscosity	$\mu_{nf} = \frac{\mu_f}{(1-\emptyset)^{2.5}}$
Electrical conductivity	$\frac{\sigma_{nf}}{\sigma_f} = 1 + \frac{3((\frac{\sigma_s}{\sigma_f}) - 1)\emptyset}{2 + (\frac{\sigma_s}{\sigma_f}) - ((\frac{\sigma_s}{\sigma_f}) - 1)\emptyset}$
Density	$\rho_{nf} = (\emptyset\left(\frac{\rho_s}{\rho_f}\right) + (1-\emptyset))\rho_f$
Thermal extension factor	$(\rho\beta)_{nf} = \left((1-\emptyset) + \emptyset\left(\frac{(\rho\beta)_s}{(\rho\beta)_f}\right)\right)(\rho\beta)_f$
Heat conductivity	$\frac{k_{nf}}{k_f} = \frac{-(m-1)\emptyset(k_f - k_s) + k_s + (m-1)k_f}{\emptyset(k_f - k_s) + k_s + (m-1)k_f}$

Heat capability $(\rho c_p)_{nf} = \left((1-\emptyset) + \emptyset\left(\frac{(\rho c_p)_s}{(\rho c_p)_f}\right)\right)(\rho c_p)_f$

The transmuted equations are as follows.

$$f''' + Wef''f''' + G_1(ff'' - (f')^2) + G_2(G_5\,\lambda\theta + Mf') + K_p f' = 0 \quad \ldots(6)$$

$$\left[R + \frac{1}{G_4}\right]\theta'' + PrG_3\,f\theta' + A^*\,\theta + MBr(f'')^2) - Pr\,G_3\,S_T f' = 0 \quad \ldots(7)$$

Transformed BCs

$$\left.\begin{aligned} f = S, f' = 1 + V_s f'', \theta = 1 + T_S\theta', \text{at}\,\eta = 0,\\ f' = 1, \theta \to 0, \text{as}\,\eta \to \infty, \end{aligned}\right\} \quad \ldots(8)$$

In spite of this, the following two significant factors have also been discussed.

Skin-friction coefficient:

$$C_{fx}Re_x^{\frac{1}{2}} = (1 + We)f''(0) \quad \ldots(9)$$

Nusselt Number:

$$Nu_x Re_x^{-\frac{1}{2}} = -(1+R)\theta'(0) \quad \ldots(10)$$

The dimensionless constraints are

$M = \frac{\sigma_f B_0{}^2}{\rho_f a}$	Magnetic field
$K_p = \frac{\nu_f}{K_0 a}$	Porosity parameter
$R = \frac{4\sigma^* T_\infty{}^3}{K^* K_f}$	Radiation parameter
$\lambda = \frac{g\,(\rho\beta)_f\,(T_w - T_\infty)}{\rho_f\,a}$	Buoyancy parameter
$We = x\Gamma\sqrt{\frac{2a^3}{\vartheta_f}}$	Williamson fluid constraint
$Pr = \frac{\vartheta_f(\rho c_p)_f}{k_f}$	Prandtl number
$Ec = \frac{u_w{}^2}{(c_p)_f(T_w - T_\infty)}$	Eckert number
$A^* = Q^*/(\rho c_p)_f a$	Heat cause/bowl constraint
$S_T = \gamma_T x/(T_w - T_\infty)$	Stratification Parameter
$A = \frac{b}{a}$	Stretching ratio Parameter
$V_s = c_1\sqrt{\frac{a}{\vartheta_f}}$	velocity slip parameter

$$G_1 = \left[\left((1-\emptyset) + \emptyset\frac{\rho_s}{\rho_f}\right)\right](1-\emptyset)^{2.5}$$

$$G_2 = (1-\emptyset)^{2.5}$$

$$G_3 = \left((1-\emptyset) + \emptyset\frac{(\rho_{c_p})_s}{(\rho_{c_p})_f}\right)$$

$$G_4 = \frac{k_s + (m-1)k_f + \emptyset(k_f - k_s)}{k_s + (m-1)k_f - (m-1)\emptyset(k_f - k_s)}$$

$$G_5 = \left((1-\emptyset) + \emptyset\frac{(\rho\beta)_s}{(\rho\beta)_f}\right)$$

Results and Discussion

The coupled nonlinear ordinary differential Eqs (6) and (7) governed by boundary conditions (8) are solved numerically using the bvp5c solver. The computed profiles illuminate the parametric dependence of momentum and thermal fields on the controlling dimensionless parameters, as presented through detailed graphical analysis below. The parameter values employed in the simulations are stated accordingly.

$We = 0.5, \lambda = 0.7, M = 2, K_p = 0.5, R = 0.3, \Pr = 7,$
$A^* = 0.2, Br = 0.5, S_T = 0.5, S = 0.8,$
$V_s = 0.5$ and $T_s = 0.5$.

Table 1 catalogues the thermophysical properties of the base fluid (water) and silver nanoparticles, both of which are fundamental inputs for accurately characterising the heat transfer behaviour of the resulting nanofluid system. Table 2 presents a quantitative validation of the present numerical results against previously published benchmark data obtained in the limiting case where additional physical

Table 1 — Thermal physical prices of base and nanofluid[37]

	$k\ (W.m^{-1}.k^{-1})$	$\rho\ (kg.m^{-3})$	$\sigma\ (S.m^{-1})$	$c_p\ (J.kg^{-1}.k^{-1})$
Ag	429	10500	$3.5\text{x}10^{6}$	235
H_2O	0.613	997.1	$5.5\text{x}10^{-6}$	4179

Table 2 — Authentication of the consequences with the prevailing works in the nonappearance of the physical parameters

Pr	Gorla and Sidawi[36]	Wang[35]	Present values
0.07	0.06562	0.0656	0.076214
0.7	0.53488	0.4539	0.521457
2.0	0.91142	0.9114	0.914462
7.0	1.89046	1.8054	1.812546

parameters are suppressed. The close correspondence between the present results and the benchmark solutions of Wang[35] and Gorla & Sidawi[36] validates the correctness of the adopted mathematical formulation and the numerical implementation, thereby establishing the reliability of the parametric results presented throughout this study.

Figs 2–3 illustrate the influence of the magnetic parameter M on the velocity and temperature profiles. As M increases, the fluid velocity undergoes a progressive reduction and the hydrodynamic boundary layer narrows correspondingly. This trend is attributed to the retarding Lorentz force induced by the transverse magnetic field, which acts in opposition to the flow direction and thus impedes nanofluid motion. Conversely, the fluid temperature and the thermal boundary layer thickness both increase with M, since the magnetic-field-induced suppression of convective transport diminishes the cooling capacity of the flow, while simultaneous Ohmic dissipation deposits additional thermal energy within the boundary layer.

Fig. 4 depicts the effect of the radiation parameter (R) on the temperature profile. Higher R augments the fluid temperature and expands the thermal boundary layer thickness, since an elevated radiative flux constitutes a supplementary energy input that reduces surface heat loss and sustains a warmer fluid region.

Fig. 5 presents the variation of the temperature profile with the thermal stratification parameter (S_T). Growing stratification progressively reduces the fluid temperature and contracts the thermal boundary layer thickness. Physically, a stronger thermal stratification establishes a stabilising vertical temperature gradient that inhibits convective heat transport in the upward direction, thereby confining the thermal boundary layer and producing a cooler near-wall fluid environment.

Fig. 6 demonstrates the effect of the Weissenberg number We on the velocity profile. Increasing We leads to an enhancement of the fluid velocity, since a larger We corresponds to more pronounced viscoelastic effects within the Williamson fluid.

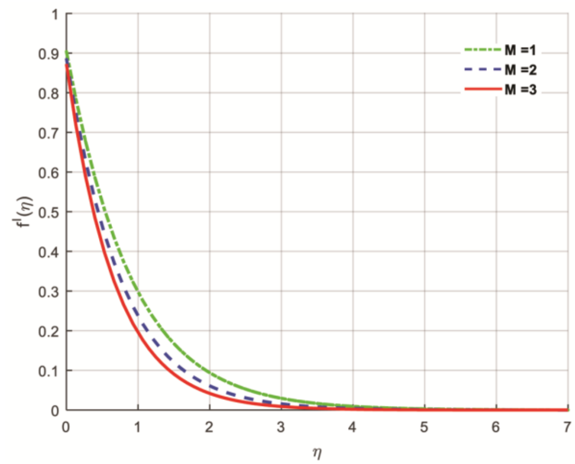

Fig. 2 — Change in $f'(\eta)$ due to M

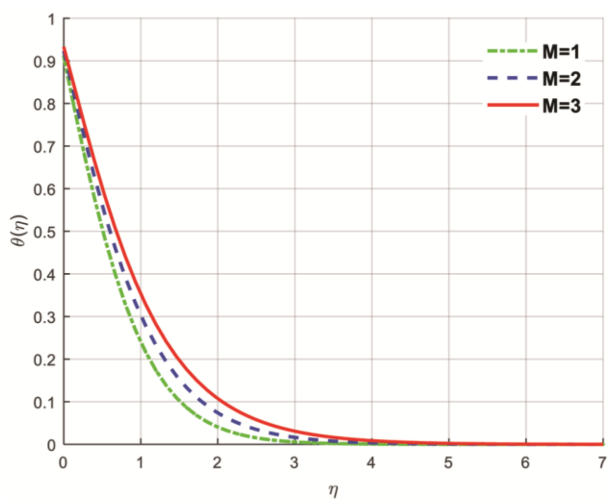

Fig. 3 — Change in $\theta(\eta)$ due to M

The associated elastic stresses store and subsequently release deformation energy, facilitating the fluid in overcoming viscous resistance and yielding elevated velocity magnitudes.

The influence of the buoyancy parameter λ on the velocity profile is illustrated in Fig. 7. An increase in λ amplifies fluid velocity, as stronger thermally-driven buoyancy forces provide an additional momentum source that supplements the stretching-induced flow and reduces the effective resistance encountered by the fluid.

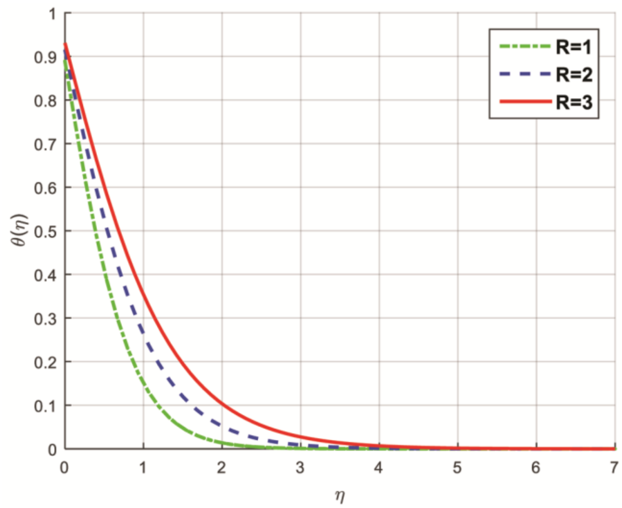

Fig. 4 — Change in $\theta(\eta)$ due to R

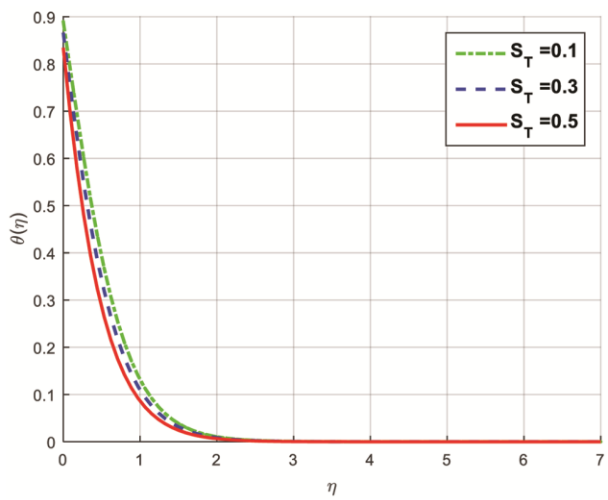

Fig. 5 — Change in $\theta(\eta)$ due to S_T

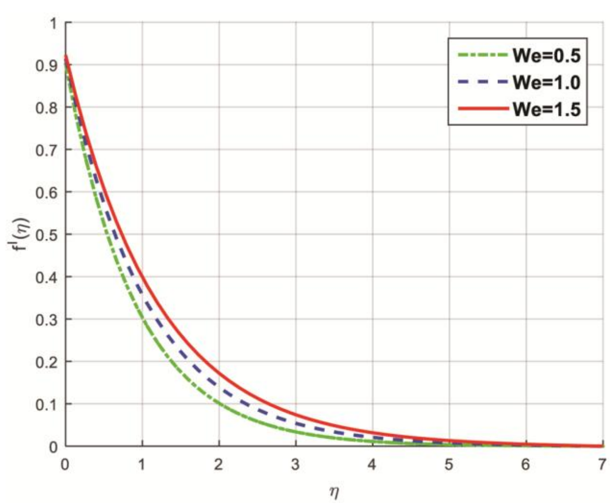

Fig. 6 — Change in $f'(\eta)$ due to We

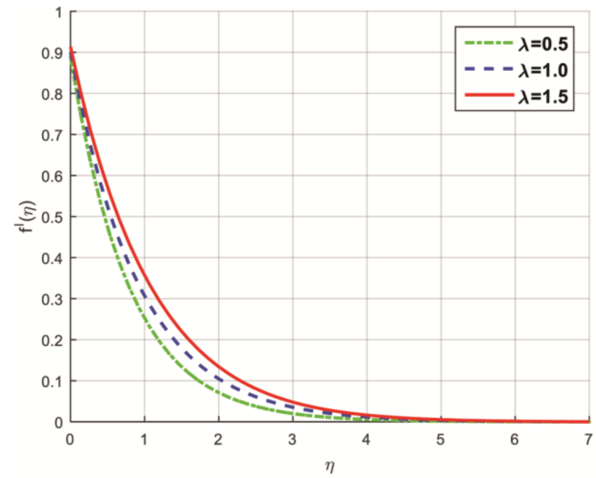

Fig. 7 — Change in $f'(\eta)$ due to λ

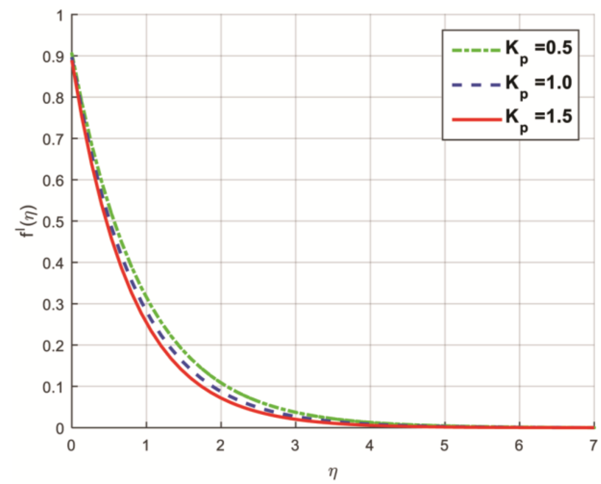

Fig. 8 —Change in $f'(\eta)$ due to K_p

Fig. 8 shows how the porosity parameter K_p affects the velocity profile. Elevating K_p diminishes the fluid velocity and compresses the hydrodynamic boundary layer. This behaviour arises because a more permeable medium exerts greater hydraulic resistance on the moving fluid; the pore network acts as distributed obstacles that extract kinetic energy from the flow and thereby decelerate it.

Fig. 9 presents the dependence of the temperature profile on the Brinkman number Br. A rise in Br produces a marked elevation in fluid temperature and a corresponding thickening of the thermal boundary layer. The underlying physical mechanism is viscous dissipation: a larger Br value reflects intensified internal frictional forces that irreversibly convert mechanical energy into thermal energy, thereby heating the fluid and enlarging the thermal layer.

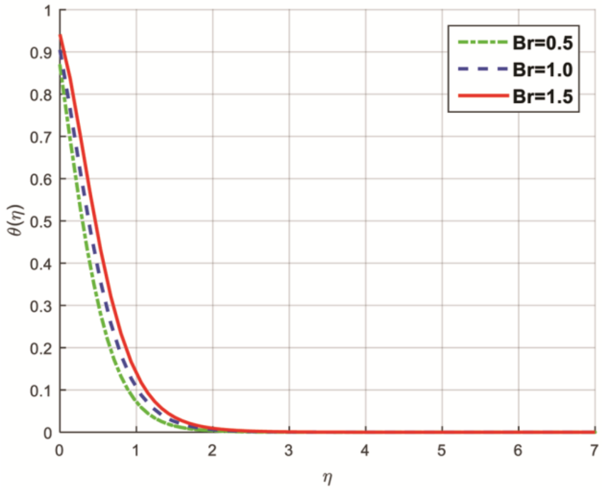

Fig. 9 — Change in $\theta(\eta)$ due to Br

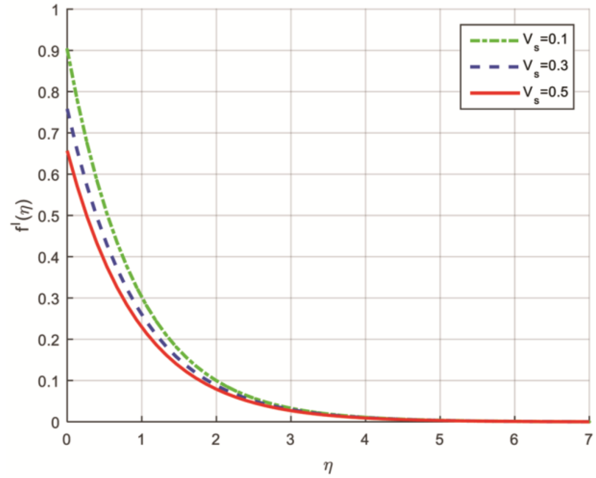

Fig. 11 — Change in $f'(\eta)$ due to V_s

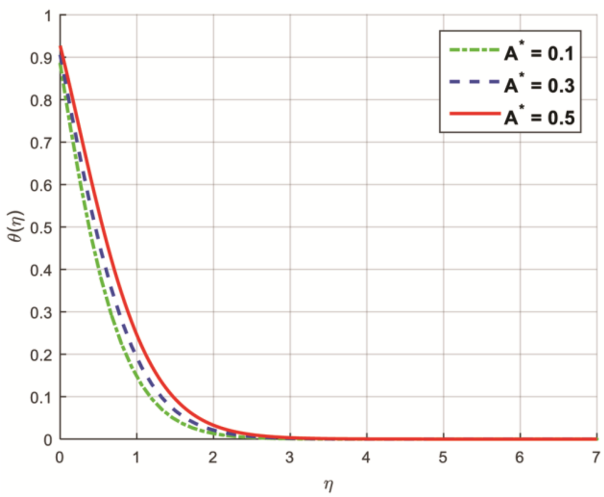

Fig. 10 — Change in $\theta(\eta)$ due to A^*

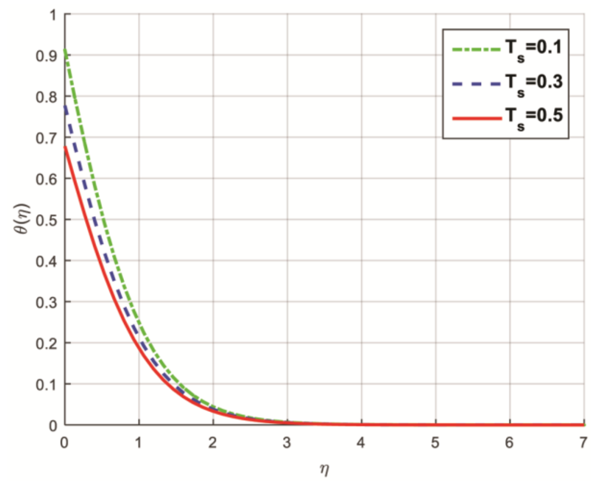

Fig. 12 — Change in $\theta(\eta)$ due to T_s

Fig. 10 illustrates the effect of the heat generation/absorption parameter A^* on the temperature distribution. When A^* is positive (heat source), external thermal energy is injected into the fluid, causing an increase in temperature and expansion of the thermal boundary layer. In contrast, a negative A^* (heat sink) extracts thermal energy from the system, lowering the fluid temperature and thinning the boundary layer. This dual behaviour directly reflects the competing thermal energy addition and removal mechanisms.

Fig. 11 depicts the influence of the velocity slip parameter V_s on the momentum profile. Increasing V_s progressively reduces the wall-tangential velocity and narrows the hydrodynamic boundary layer. This is a consequence of the partial-slip boundary condition: the fluid undergoes relative sliding motion along the wall rather than adhering completely to it, resulting in diminished near-wall momentum exchange and a correspondingly thinner velocity boundary layer.

Fig. 12 presents the effect of the thermal slip parameter T_s on the temperature profile. A higher T_s value reduces the fluid temperature and thins the thermal boundary layer, since thermal slip attenuates the heat exchange between the solid wall and the adjacent fluid layer. The resulting reduction in wall-to-fluid heat transfer prevents effective thermal loading of the fluid, yielding lower temperatures throughout the boundary layer.

Figs 13 and 14 examine the role of the nanoparticle volume fraction ϕ on the velocity and temperature

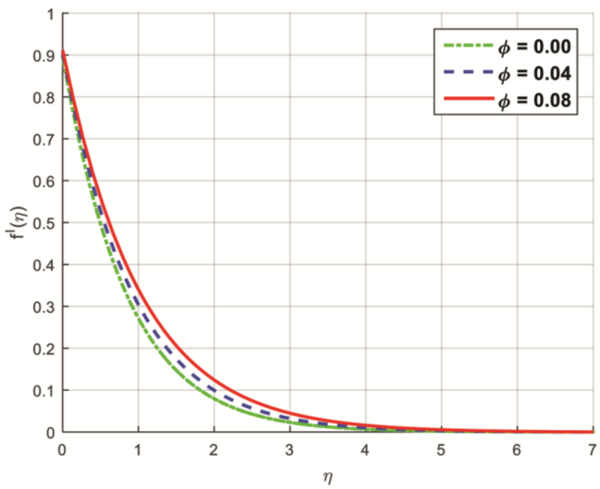

Fig. 13 — Change in $f'(\eta)$ due to ϕ

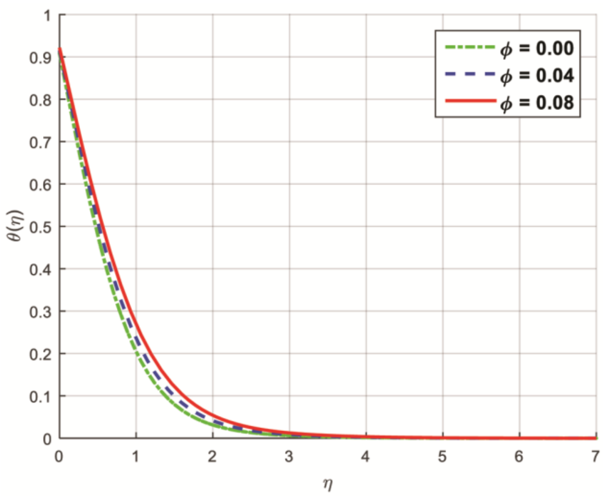

Fig. 14 — Change in $\theta(\eta)$ due to ϕ

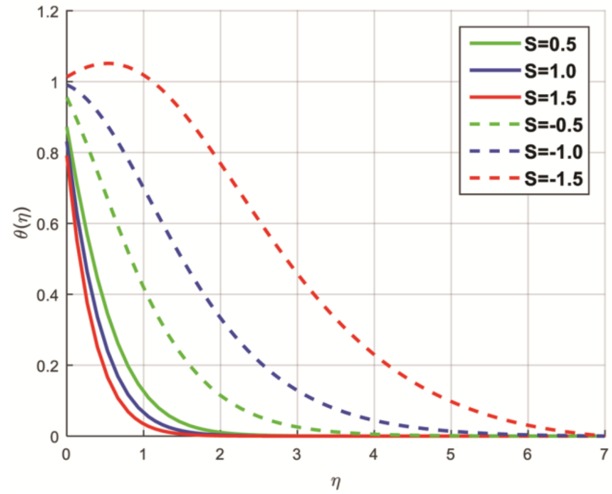

Fig. 15 — Change in $\theta(\eta)$ due to S

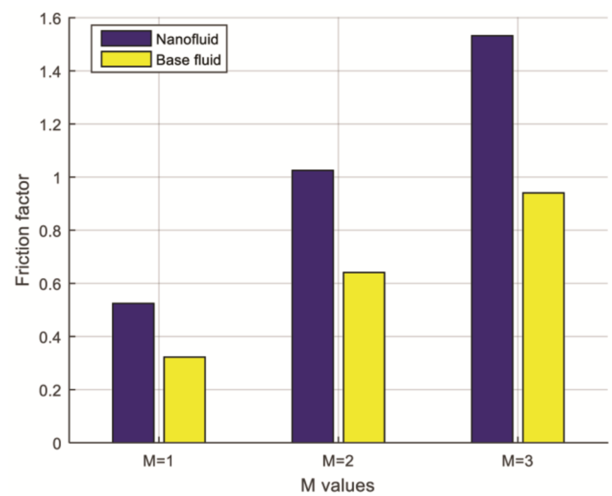

Fig. 16 — Sway of M on Friction factor

distributions for Ag–H_2O nanofluid. Both profiles intensify with increasing ϕ, reflecting the dual effect of nanoparticle loading: the enhanced effective thermal conductivity accelerates thermal diffusion across the boundary layer, while the elevated effective viscosity modifies the momentum distribution, collectively broadening both boundary layer thicknesses.

Fig. 15 displays the influence of the suction/injection parameter S on the temperature profile. Under suction ($S > 0$), thermal energy is continuously extracted as heated near-wall fluid is drawn away, thinning the thermal boundary layer and reducing the local temperature. Under blowing ($S < 0$), cooler ambient fluid is introduced at the surface, which dilutes the thermal energy and similarly suppresses the temperature. Although both mechanisms attenuate excessive thermal boundary layer growth, they operate through fundamentally distinct physical pathways: one by extracting fluid mass and the other by supplying thermally cooler fluid.

Figs 16–21 present the combined influence of M, R and S_T on the skin friction coefficient and local Nusselt number for both the nanofluid and pure base fluid cases. In all cases, augmenting each parameter results in a monotonic increase in both engineering quantities. Physically, an intensified magnetic field amplifies the Lorentz drag on the fluid, elevating near-wall shear stress and consequently the skin friction factor. Correspondingly, larger radiation parameter and stronger thermal stratification enhance the overall energy transfer rate within the fluid, steepening the wall temperature gradient and thereby raising the Nusselt number. In the nanofluid

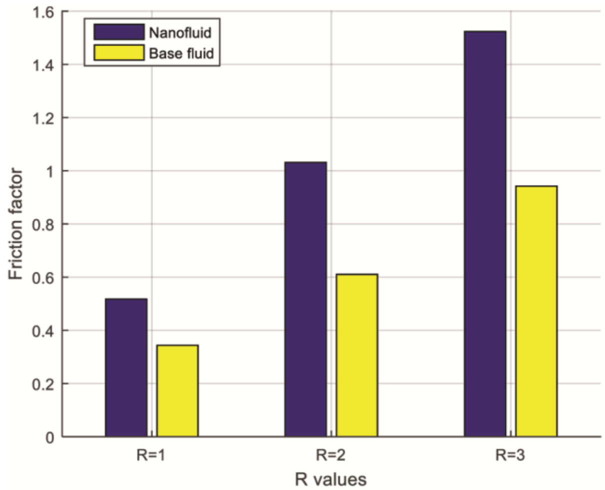

Fig. 17 — Sway of R on Friction factor

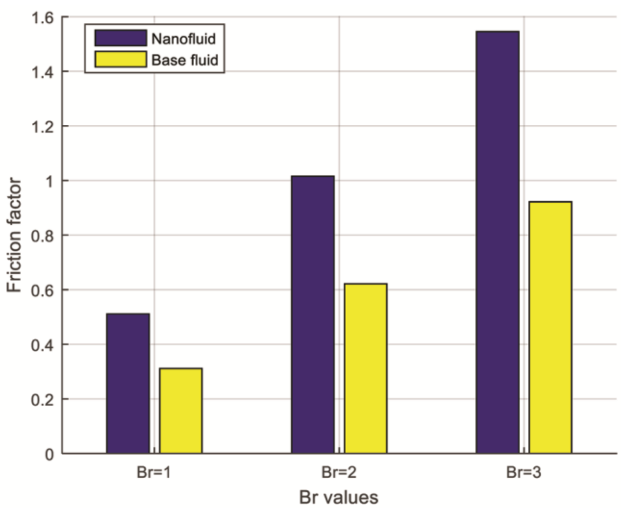

Fig. 18 — Sway of Br on Friction factor

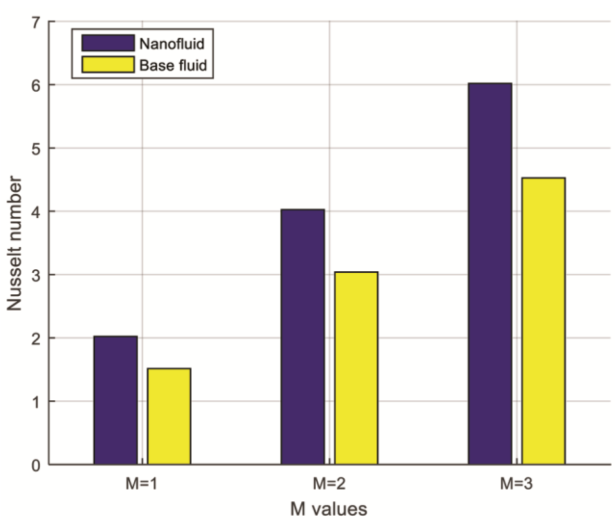

Fig. 19 — Sway of M on Nusselt number

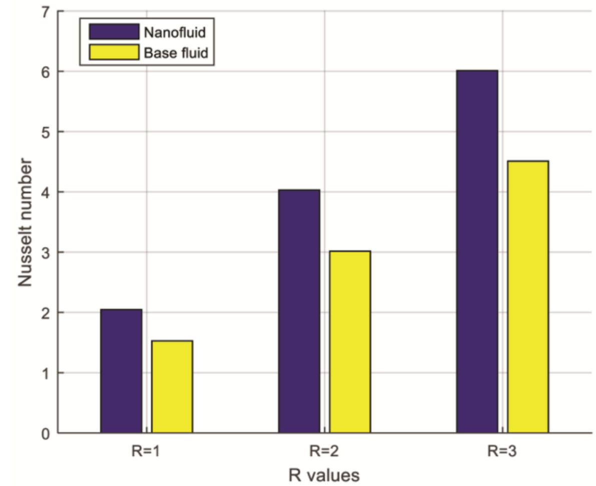

Fig. 20 — Sway of R on Nusselt number

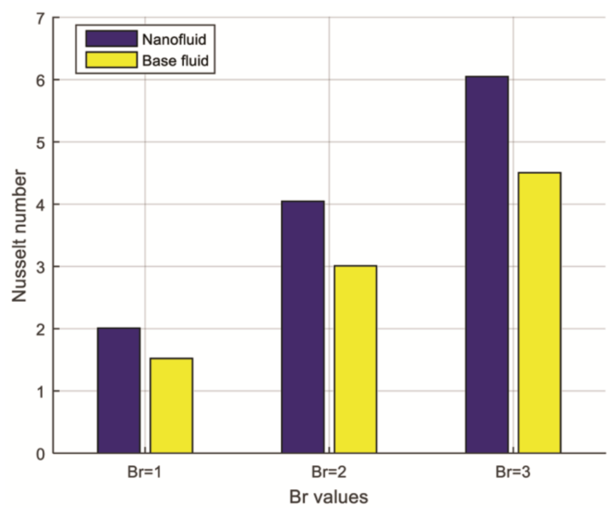

Fig. 21 — Sway of Br on Nusselt number

configuration, the presence of suspended silver nanoparticles significantly augments the effective thermal conductivity, enabling more efficient heat convection at the wall and producing a consistently higher Nusselt number relative to the pure base fluid. This superior thermal performance of the nanofluid is consistently demonstrated across all parametric cases examined.

Conclusion

This study presents a comprehensive theoretical investigation of heat transport characteristics in thermally stratified Williamson nanofluid flow over a porous stretching surface, with due consideration of thermal radiation, Ohmic heating, and internal heat generation or absorption effects. Silver–water (Ag–H_2O) nanofluid is selected as the working medium owing to its well-documented superior thermal conductivity and extensive applicability in modern thermal engineering systems. Appropriate similarity transformations are employed to convert the nonlinear governing conservation equations into a dimensionless ODE system, which is then solved numerically to explore the combined parametric effects on flow and heat transfer characteristics. The computed results are systematically presented through graphical profiles to provide clear physical insight into the velocity and temperature responses under varying parametric conditions.

- Application of a transverse magnetic field induces retarding Lorentz forces that progressively decelerate fluid motion while simultaneously intensifying thermal energy accumulation within the boundary layer, a dual effect exploitable in electromagnetic flow regulation and precision thermal management systems.
- Thermal radiation and internally generated heat jointly elevate the fluid temperature by supplementing the energy transport mechanisms within the boundary layer, with direct beneficial implications for concentrated solar collector performance and thermal reactor efficiency.
- The viscoelastic character of the Williamson fluid, acting synergistically with thermally-driven buoyancy, reinforces momentum transport and stabilises the flow field, attributes that are particularly beneficial in polymeric extrusion, physiological flow modelling, and natural convection cooling systems.
- The dispersion of silver nanoparticles markedly elevates both the effective thermal conductivity and convective heat transfer coefficient of the base fluid, yielding superior cooling efficiency and rendering Ag–H_2O nanofluids highly suitable for high-performance electronic thermal management and renewable energy applications.
- Boundary velocity slip and porous medium permeability collectively modulate near-wall momentum transfer and thermal exchange, findings that carry direct engineering relevance for tribological lubrication systems, industrial filtration processes, and porous channel-based cooling architectures.

Acknowledgments

The authors sincerely acknowledge their respective institutions for the support provided in conducting this research.

Conflict of Interest

The authors declare no conflict of interest.

References

1 Akbar N S, Nadeem S & Lee C, Influence of heat transfer and chemical reactions on Williamson fluid model for blood flow through a tapered artery with a stenosis, *Asian J Chem*, 24 (2012) 2433.

2 Zeeshan A & Ellahi R, Effect of slip, Hall current, and radiation on non-Newtonian nanofluid flow over a stretching surface, *Int J Numer Methods Heat Fluid Flow*, 28 (2018) 1462.

3 Olkha A & Kumar M, Heat transfer characteristics in Williamson fluid flow in a vertical channel with chemical reaction and entropy production, *Energy Storage Convers*, 2 (2024) 515.

4 Zeeshan A, Arain M B, Bhatti M M, Alzahrani F & Bég O A, Radiative bioconvection nanofluid squeezing flow between rotating circular plates: Semi-numerical study with the DTM Padé approach, *Mod Phys Lett B*, 36 (2022) 2150552.

5 Abbas A, Khan A, Abdeljawad T & Aslam M, Numerical simulation of variable density and magnetohydrodynamics effects on heat generating and dissipating Williamson Sakiadis flow in a porous space: Impact of solar radiation and Joule heating, *Heliyon*, 9 (2023) e20349

6 Ashwinkumar G P, Heat and mass transfer analysis in unsteady MHD flow of aluminum alloy/silver-water nanoliquid due to an elongated surface, *Heat Transf*, 50 (2021) 1679.

7 Sulochana C, Savita & Ashwinkumar G P, Joule heating effect on the MHD flow of tangent hyperbolic mixed nanofluid embedded with MgO and CuO nanoparticles, *Int J Ambient Energy*, 44 (2023) 1904.

8 Anantha Kumar K, Reddy B R & Venkata Ramudu A C, MHD Cattaneo-Christov flow of Casson nanofluid over a porous surface: A solar application, *Mod Phys Lett B*, 39 (2025) 2550231.

9 Ashwinkumar G P, Computational analysis on MHD Sakiadis flow of hybrid nanoliquid past an incessantly moving thin needle, *Int J Model Simul*, 45 (2025) 454.

10 Mondal S, Ghosh R & Sharma R P, Entropy generation effects on hydromagnetic Williamson nanofluid flow through a porous media, *Nanosci Nanotechnol Asia*, 13 (2023) 9.

11 Raju C S K & Sandeep N, Heat and mass transfer in MHD non-Newtonian bio-convection flow over a rotating cone/plate with cross diffusion, *J Mol Liq*, 215 (2016) 115.

12 Rasool G, Zhang T, Chamkha A J, Shafiq A, Tlili I & Shahzadi G, Entropy generation and consequences of binary chemical reaction on MHD Darcy-Forchheimer Williamson nanofluid flow over a non-linearly stretching surface, *Entropy*, 22 (2020) 18.

13 Khana A Y, Oyelakin I S, Mondal S & Dey S, Entropy approach of hydromagnetic Williamson nanofluid flow with Joule heating, *Int J Ambient Energy*, 44 (2022) 1106.

14 Sharma R P, Baag S, Sahoo P & Mishra S R, On the radiative heat transport phenomena in MHD Williamson nanofluid flow past an expanding surface with an interaction of inclined magnetic field, *J Therm Anal Calorim*, 148 (2023) 7319.

15 Sandeep N, Lingamurthy S, Shukla S & Anantha Kumar K, Significance of nanolayers in enhanced thermal conductivity

of nanofluid: An application for solar energy optimization, *J Therm Anal Calorim*, 151 (2026) 1805.
16 Sheikholeslami M & Ganji D D, Magnetohydrodynamic nanofluid flow and heat transfer using CVFEM in a porous medium considering radiation, *J Mol Liq*, 222 (2016) 618.
17 Sulochana C & Ashwinkumar G P, Impact of Brownian motion and thermophoresis on magnetohydrodynamic flow of magnetic nanofluid past an elongated sheet in the presence of thermal diffusion, *Multidiscip Model Mater Struct*, 14 (2018) 744.
18 Ashwinkumar G P & Sulochana C, Effect of radiation absorption and buoyancy force on the MHD mixed convection flow of Casson nanofluid embedded with $Al_{50}Cu_{50}$ alloy nanoparticles, *Multidiscip Model Mater Struct*, 14 (2018) 1082.
19 Lone S H, Thakur S K & Tripathi D, Comparative analysis of hybrid and mono nanofluids in the presence of radiation and magnetic field: A numerical approach, *Int Commun Heat Mass Transf*, 135 (2022) 106014.
20 Nisar Z, Ahmed B, Ghazwani H A, Muhammad K, Hussien M & Aziz A, Numerical study for bioconvection peristaltic flow of Sisko nanofluid with Joule heating and thermal radiation, *Heliyon*, 9 (2023) e22505.
21 El-Hakiem M A, Mustafa M & Abo-Dahab S M, Radiation, velocity and thermal slip effects toward MHD boundary-layer flow through heat and mass transport of Williamson nanofluid with porous medium, *Arab J Sci Eng*, 47 (2022) 16355.
22 Rashad A M, Nafe M A & Eisa D A, Heat variation on MHD Williamson hybrid nanofluid flow with convective boundary condition and Ohmic heating in a porous material, *Sci Rep*, 13 (2023) 6071.
23 Rawat S K, Yaseen M, Khan U, Kumar M, Eldin S M, Alotaibi A M & Galal A M, Significance of non-uniform heat source/sink and Cattaneo-Christov model on hybrid nanofluid flow in a Darcy-Forchheimer porous medium between two parallel rotating disks, *Front Mater*, 9 (2023) 1097057.
24 Yasmin H, Bossly R, Alduais F S, Al-Bossly A & Saeed A, Analysis of radiated ternary hybrid nanofluid flow containing TiO_2, $CoFe_2O_4$ and MgO nanoparticles past a bi-directional extending sheet using thermal convective and velocity slip conditions, *AIMS Math*, 10 (2025) 9563.
25 Kayalvizhi J & Kumar A G V, Entropy analysis of electromagnetohydrodynamic hybrid nanofluid stagnation-point flow over a porous stretching sheet with melting heat transfer in the presence of thermal radiation, *Energies*, 15 (2022) 8317.
26 Kazmi S N, Abbasi F M & Shehzad S A, Entropy generation for hybrid nanofluid mobilized by peristalsis with inclined magnetic field, *Proc Appl Math*, 16 (2024) 1.
27 Shah Z, Kumam P & Deebani W, Radiative MHD Casson nanofluid flow with activation energy and chemical reaction over a nonlinearly stretching surface through entropy generation, *Sci Rep*, 10 (2020) 4402.
28 Shah S, Atif S M & Kamran A, Radiation and slip effects on MHD Maxwell nanofluid flow over an inclined surface with chemical reaction, *Heat Transf*, 50 (2021) 4062.
29 Abbas A, Ahmad H, Mumtaz M, Ilyas A & Hussan M, MHD dissipative micropolar fluid flow past stretching sheet with heat generation and slip effects, *Waves Random Complex Media*, 35 (2022) 6284.
30 Akbar N S, Khan Z H & Nadeem S, Slip effects on Carreau nanofluid past a stretching sheet, *Appl Math Comput*, 237 (2014) 249.
31 Kumar K A, Sugunamma V & Sandeep N, Numerical exploration of MHD radiative micropolar liquid flow driven by stretching sheet with primary slip: A comparative study, *J Non-Equilib Thermodyn*, 44 (2019) 101.
32 Kumar K A, Sugunamma V, Sandeep N & Reddy J V R, Impact of Brownian motion and thermophoresis on bioconvective flow of nanoliquids past a variable thickness surface with slip effects, *Multidiscip Model Mater Struct*, 15 (2019) 103.
33 Raju S K, Sugunamma V & Reddy B N, Slip and Joule heating effects on hybrid nanofluid over a vertical medium, *Heat Transf*, 50 (2021) 5533.
34 Sandeep N, Lingamurthy S & Kumar K A, Optimal usage of solar energy in cylindrical film flow of prandtl ferrofluid: A relative analysis of Hamilton-crosser and Xue nano models, *Multidiscip Model Mater Struct*, 22 (2025) 610.
35 Wang C Y, Free convection on a vertical stretching surface, *ZAMM J Appl Math Mech*, 69 (1989) 418.
36 Reddy G R S & Sidawi I, Free convection on a vertical stretching surface with suction and blowing, *Appl Sci Res*, 52 (1994) 247.
37 Acharya N, Das K & Kumar K P, Ramification of variable thickness on MHD TiO_2 and Ag nanofluid flow over a slendering stretching sheet using NDM, *Eur Phys J Plus*, 131 (2016) 303.